# Modelling of RC beams strengthened with TRM in Shear

Mohamed A. Sakr[1]; Ayman A. Sleemah[1]; Tarek M. Khalifa[1]; and Mohamed Ali[2]

**Abstract**: Textile-reinforced mortar systems are composed of high-strength textiles that are embedded in mortar matrix. This paper presents a 2D non-linear finite element model (FEM). Moreover, a new model to simulate the de-bonding failure between TRM and the concrete substrate was developed. This model based on the experimentally-available bond-slip data that are depended on the degree of surface roughness. The proposed model verified with literature. The comparison between numerical and experimental results demonstrated that the FEM is able to simulate the overall response and capture different failure modes with a good agreement. Furthermore, the validated FEM was used to investigate the effect of different parameters on the overall behavior of the strengthened RC simple beams. These parameters included mortar thickness, fiber type and number of TRM layers.

**Author keywords**: TRM; Reinforced Concrete beams; Shear strengthening; Finite-element model; Modelling.

[1]Department of Structural Engineering, Tanta University, Tanta, Egypt
[2]Faculty of Civil Engineering, Tanta University, Tanta, Egypt
Correspondence

Mohamed Ali, Faculty of civil
Engineering, Tanta University, Tanta, Egypt.
Email: engmuhamedali@yahoo.com

## 1 Introduction

One of the most common upgrading techniques for reinforced concrete members involves the use of fiber-reinforced polymer (FRP) jackets, which are aimed at increasing the shear resistance in regions with inadequate transverse reinforcement. The use of FRP has gained increasing popularity in the civil engineering community, because of the favorable properties possessed by these materials, namely: extremely high strength-to-weight ratio, corrosion resistance, ease and speed of application, and minimal change in the geometry [1]. Despite all these advantages, the FRP strengthening technique has a few disadvantages, which are attributed to the resins used to bind or impregnate the fibers [2,3]. These drawbacks may include: (1) debonding of FRP from the concrete substrate; (2) poor behavior of epoxy resins at temperatures above the glass transition temperature; (3) relatively high cost of epoxies; (4) inability to apply FRP on wet surfaces or at low temperatures; (5) weakness of steam permeability, that may cause damage to the concrete structure; (6) incompatibility of epoxy resins and substrate materials; and (7) difficulty to conduct Post earthquake estimation of the damage suffered by the reinforced concrete behind (undamaged) FRP jackets. One possible solution to the previously listed problems would be the replacement of organic with inorganic binders, e.g., cement-based mortars, leading to the replacement of FRP with fiber-

reinforced mortars (FRM). The characteristics of TRM systems subjected to direct tensile forces have been the focus of many studies [4,5,6,7,8,9]. Colombo et al. (2013) [10] investigated the effect of the fabric geometry (warp and weft spacing and cross section), the loading rate, and the curing method on the tensile strength and ductility of the TRM system. It was concluded that the bonded surface of the warp roving strongly influenced the strength of the system, while the weft roving controlled the cracking distance and the overall ductility of the system. Curing conditions also affected the matrix shrinkage and consequently, the strength and mode of failure of the system. The higher strength was achieved when the systems were cured for 28 days at room temperature. The researchers also reported on the loss of strength and ductility while decreasing the displacement rate during testing. Blanksvärd et al. (2009) [11] compared the effectiveness of TRM and TRP strengthening systems using carbon fabrics. The beams had rectangular cross section of 180 mm × 500 mm, and were 4500 mm long. Test results showed that the TRM system increased the load capacity by up to 97%, relative to control un-strengthened specimen, and the failure mode was by rupture of the carbon fibers. The TRP system increased the load capacity of the tested beams by 104% and failed by debonding. Si Larbi et al. (2010) [12] tested beams with rectangular section of 150 × 220 mm and 570 mm span between supports were tested. TRM and TRP reinforcement were applied as U-shaped jackets. Results from the study revealed

that TRP strengthening led to a strength gain of 22%, relative to a control unstrengthened specimen, while the TRM strengthening systems resulted in a strength gain of up to 69%. Thus, the TRP jacket was less effective in enhancing the strength of the specimen in this case. These results may be misleading because only one TRP-strengthened specimen was fabricated, whereas there were three TRM-strengthened specimens with different configurations. Adel younis and Usama Ebead et al. (2018) [13] studied the effectiveness of fabric reinforced cementitious matrix (FRCM) systems in shear-strengthening of reinforced concrete beams. Three types of FRCM systems were investigated, namely, polyparaphenylene benzobisoxazole (PBO)-FRCM, Carbon-FRCM, and Glass-FRCM. Seven 2100-mm long, 150-mm wide, and 330-mm deep reinforced concrete simply supported beams were tested. FRCM has been successfully improved the load carrying capacity of shear critical RC beams. The average increase in the load carrying capacity acquired with FRCM-strengthening was 57%. Yousef Al-Salloum et al. (2012)[14] tested beams with rectangular section of 150 x 200 mm and 1500 mm span between supports were tested. The basalt textile-reinforced mortar layers increased the shear capacity of reinforced concrete beams from 36–88%. The results showed that the shear resistance increased as the number of TRM layers increased from two to four per side. Because of the weakness of the basalt textile used in this research, the number of layers used (two and four layers per side)

4

did not prevent the sudden shear failure. Also, two mortar types were compared in TRM strengthening of RC beams: cementitious mortar and polymer-modified mortar. Experimental results showed that there was no significant difference in the mortars when two layers of TRM are applied. However, with four layers of TRM, the specimens with polymer-modified mortar had ultimate loads which were 16%, on average, more than those with two layers of TRM.

In the present study, a numerical analysis of the performance of the RC simple beams strengthened with TRM using 2D non-linear finite element model (FEM). Moreover, a new model to simulate the de-bonding failure between TRM and the concrete substrate was developed. The proposed model verified with literature. Furthermore, the validated FEM was used to investigate the effect of different parameters on the overall behavior of the strengthened RC simple beams. These parameters included mortar strength, fiber type and number of TRM layers.

## 2 Finite element model

Currently, the finite element modeling (FEM) of strengthening using textile reinforced mortar are very limited and all of them used 3D modeling which consume very long time and effort. In order to fill this gap in knowledge, a 2D nonlinear FEM has been developed using Abaqus/standard package [21]. This model was validated by comparing the obtained

load–deflection response, ultimate load and failure mode with the experimental results. The model was validated with experimental control RC beam and beams strengthened with TRM tested by Al-Saloum et al. (2012)[14] under monotonic loading that failed due to shear.

**2.1 Material properties and constitutive models**

## 2.1.1 Concrete and mortar

There are several constitutive models available in Abaqus to characterize the behavior of plain concrete or mortar subjected to varying conditions of loading. These include the Smeared Crack model, the Brittle Cracking model and the Concrete Damage Plasticity (CDP) model. The smeared Crack model is usually used in case of simulating the behavior of reinforced or unreinforced concrete under low confining pressure subjected to monotonic loading. The Brittle Crack model used to simulate concrete when the compressive behavior remains elastic and the nonlinearity of material becomes from tensile cracking. Finally, the CDP model can simulate the cyclic response of concrete experiencing damage in both tension and compression. In the current study, the CDP model was used to simulate the nonlinear mechanism of both concrete and mortar. The CDP model is based on the yield functions proposed by Lubliner [15]. and modified by Lee and Fenves [16]. It assumes that the main two failure mechanisms are tensile cracking and compressive crushing. This model requires some input data to simulate concrete uniaxial stress-strain properties and these

parameters include; The uniaxial properties of concrete when subjected to tension and compression in terms of stress-strain and modulus of elasticity, Poisson's ratio and it assumed to be 0.2 for both concrete and mortar, the dilatation angle that determines the direction of the plastic flow through the incremental plastic strain vector ($\psi$), the flow potential eccentricity (the default value being 0.1), the ratio of initial equibiaxial compressive yield stress to initial uniaxial compressive stress, $\sigma_{bo}/\sigma_{co}$ (the default value being 1.16), The viscosity parameter, $\mu$, The ratio of the second stress invariant on the tensile meridian to that on the compressive meridian at initial yield for any given value of the pressure invariant such that the maximum principal stress is negative $K_c$ (The default value being 0.667).

- The model in compression

The uniaxial stress-strain relationship in compression proposed by Saenz [17] was used in this study as reported in Hu and Schnobrich [18]. The relation assumed to be initially linear until micro crack initiation so the behavior becomes nonlinear as shown in Figure 1(a).

7
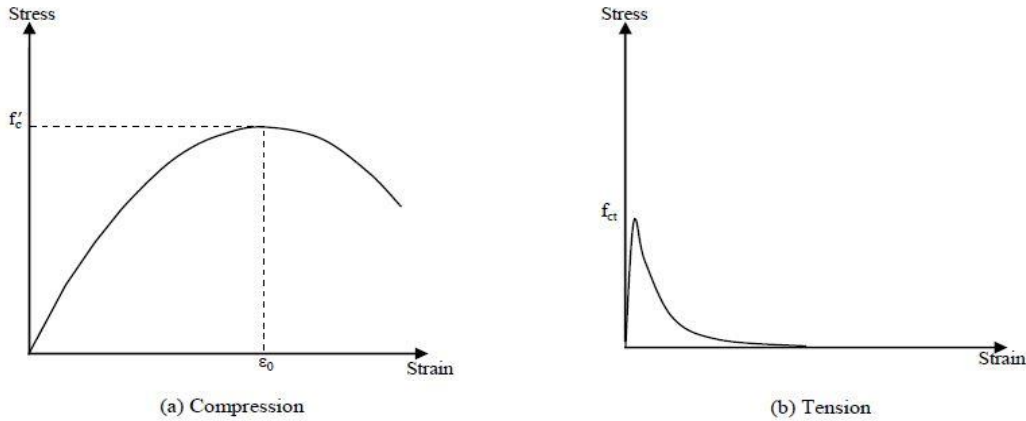
**Figure 1** Uniaxial stress-strain curves of concrete and mortar

- The model in tension

The stress-strain response of concrete under uniaxial tension is also follows the same

manner of the compressive curve. It displays two distinct zones, namely the elastic zone

and the softening zone as shown in Figure 1(b). In order to define the elastic region, the

elastic modulus, Ec and the tensile strength Fct are required and they can be calculated

according to the ACI code as sown in equation (1), (2).

- $E_c = 4700\sqrt{\bar{f}_{cy}}$          Equation. 1

- $f_{ct} = 0.33\sqrt{\bar{f}_{cy}}$          Equation. 2

where $\bar{f}_{cy}$ is the cylinder compressive of strength. After reaching the failure stress, the

8

formation of micro-cracks is presented with softening stress-strain response. In the current study, fracture energy cracking criterion is used to simulate tension softening of concrete according to the model of Hillerborg [19] as shown in Figure 2, where Gf is the fracture energy of concrete.
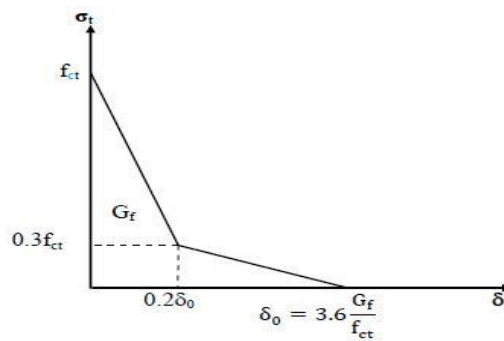


**Figure 2** Softening curve of concrete under uni-axial tension.

## 2.1.2 Reinforced steel

Under monotonic loading the steel is assumed to be bilinear elastic-plastic material and identical in tension and compression and in this study it is assumed to be elastic-perfectly material . The elastic modulus, Es, the yield stress, σy , and the ultimate stress σu  are the values needed to draw the stress strain curve for the RFT steel as shown in Figure 3. A Poisson's ratio of 0.3 was used for the steel reinforcement. The bond between reinforcement steel and concrete was assumed as a perfect bond.

9
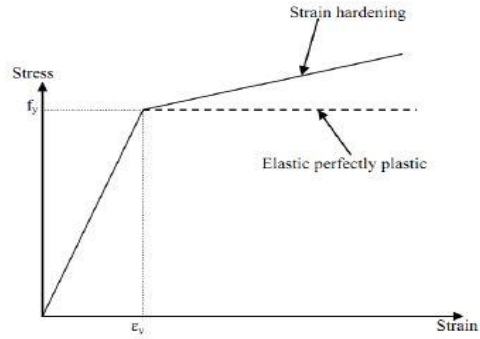
**Figure 3** Idealized stress-strain relationship for reinforcing steel

## 2.1.3 Textile or fibers

Initially, the matrix and fibers deform elastically. Eventually, the matrix yields and deforms plastically as mentioned before but the fibers continue to stretch elastically John Wiley et.al 2012 [20]. These relationships give rise to the nearly linear elastic characteristic stress-strain curve shown in Figure 4. Hence, the textiles or fibers is considered as linear elastic isotropic until sudden tension failure.
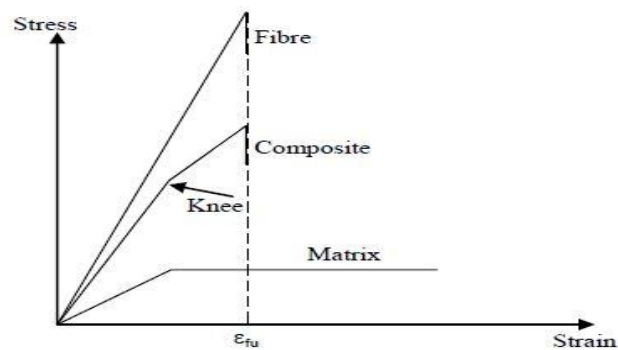


**Figure 4** Stress-strain curves for textile, matrix and TRM composite

10

## 2.1.4 Contact modelling

There are three types of contact in FEM, the contact between steel and concrete, the contact between textile and mortar, and the contact between the TRM composite and concrete substrate. The interaction between the reinforcement and concrete is assumed to be fully bonded and modeled using the embedded region constraint. The contact between the textile and the mortar is assumed to be fully bonded as for the last researches this type of failure didn't occur except in testing composite properties in direct tension tests or shear tests. For modelling the contact between TRM composite and concrete substrate, Abaqus/CAE used the traction-separation law in order to allow the debonding failure to occur. It provides three techniques for this purpose, the first is by using a cohesive element and the second depends on using a surface based cohesive behavior and the third by node to node contact. Surface-based cohesive is suitable for cases in which the interface thickness is negligibly small. If the interface adhesive layer has a finite thickness and macroscopic properties (such as stiffness and strength) of the adhesive material are available, it may be more appropriate to model the response using conventional cohesive elements.  Figure 5 shows a graphic interpretation of a simple bilinear traction–separation law written in terms of the effective tractions and effective opening displacement and it consist from three parts, The first part is initially illustrates the linear elastic traction separation, while the second part is

the damage initiation point, and the third part is the damage evaluation zone. It is obvious that the relationship between the traction stress and effective opening displacement is defined by the stiffness, K, the local strength of the material, τmax or σmax, a characteristic opening displacement at fracture, δf, or the energy needed for opening the crack, Gcr, which is equal to the area under the traction–displacement curve. Modeling of the failure at the interface between substrate and jacket concrete requires two stages: (i) damage initiation, and (ii) damage evaluation. The first stage (damage initiation) indicates a critical cohesive response where the stiffness of the interface starts to degrade, while the second stage (damage evolution) indicates how the interface stiffness degrades. Equation (3), provides an upper limit for the maximum shear stress τmax that depends on the roughness of the interface.

$$\tau = c. \, f_{ct} + \boldsymbol{\mu}. \, \sigma_n \quad \text{Equation. 3}$$

c and μ are factors that depend on the degree of roughness at the substrate layer, Fct and σn are the core concrete tensile stress and the normal stress. The value of the normal stress used for this study were σn = minimum tensile strength between concrete and mortar.
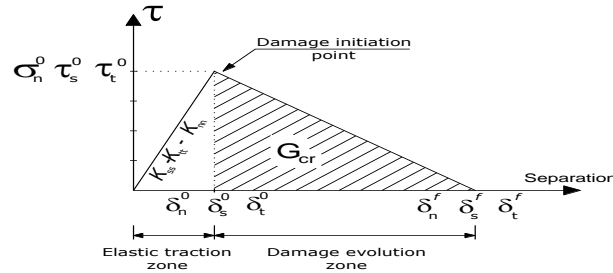
**Figure 5** Description of the traction-separationbehaviour

## 2.1.5 Node-to-node contact element (2D model)

For the 2D model, in Abaqus the shell is not considered as a surface, while the interaction in the model is between the shell of the concrete and the mortar shell and between the mortar shell and the textile shell, therefore another interaction method should be utilized. Abaqus provides node-to-node interaction method using Cartesian connector element, as shown in Figure 6 Cartesian connector element connects between two nodes allowing independent behavior in three local Cartesian directions that follow the system at node a. To define the connection type Cartesian in the present model, the normal and tangential mechanical behavior must be defined. For the normal behavior, one can define spring-like elasticity behavior for the available components of relative motion. It was assumed as a rigid link connecting point a to point b along a-b direction (U3 direction), Figure 6.

13
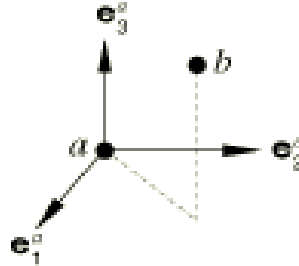
**Figure 6** Connection type CARTESIAN

For the tangential behavior, the U1, U2 direction was defined as the slip direction (perpendicular to U3 direction), and defined the tangential behavior using the cohesive parameters multiplied by area of the mesh. To represent the de-bonding failure, two layers of 2D shell elements were used, the first layer represents the concrete thickness and the second layer represents the TRM composite total thickness. The sets of connectors that used connect between the first and the second layer and represents the minimum behavior in shear between concrete and mortar to capture de-bonding mode failure.

## 2.1.6 Elements, meshing, and boundary conditions

A linear plane stress rectangular (CPS4R) or triangular (CPS3) element with reduced integration with hourglass control elements element was used for the concrete or mortar or textile as shown in Figure 7. And for the reinforcement steel a 2-node linear 2-D truss (T2D2) element was used and the same element was used for textile in the third direction that used for strengthening the lower side of beam.

14
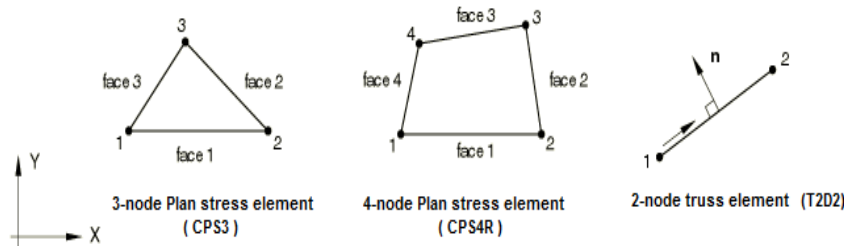
**Figure 7** Elements used in the 2D modeling

# 3 Verification of the model with previous work

Al-Salloum et al (2012) [14] experimentally used a basalt based textile for strengthening RC beams to increase their shear capacity. Two different types of mortars were used included, cementitious and polymer modified mortar. The number of textiles and the orientation of the textile were studied. Details of test beams are shown in Figure 8 and the test matrix is shown in Table 1 for the verified specimens.

## 3.1 properties of materials

The average compressive strength, fc' was in the experimental work measured to be 20 MPa and Poisson's ratio was assumed to be 0.20 for concrete. The average values for yield and tensile strengths of the longitudinal reinforcement (16mm Diameter) are 578Mpa and 684Mpa respectively, 280Mpa and 372Mpa respectively for transversal reinforcement (6mm Diameter). A Poisson's ratio of 0.3 was used and the elastic modulus was assumed to be Es=200000 for steel reinforcement. The mechanical properties of the cementitious

mortar used in this study was 2.77MPa, 23.9MPa for tensile and compressive strength respectively. Basalt-based textile was used in this study and its mechanical properties (elastic modulus = 31.94 GPa , Tensile strength = 623MPa , Nominal thickness per layer = 0.064 mm).
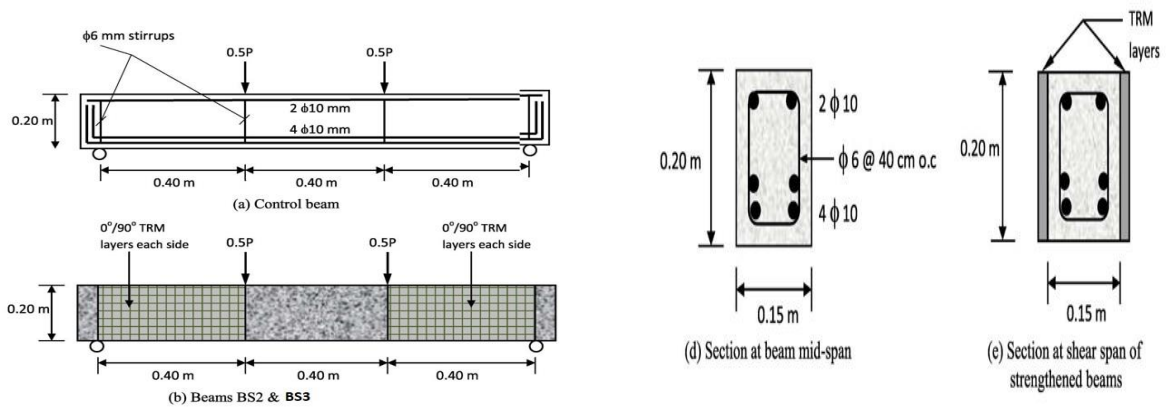


**Figure 8** Dimensions and R.F.T details of the tested beams.

**Table 1** Test matrix

| Specimen ID | Mortar type | Number of TRM layers each side | Textile orientation | Number of specimens |
|---|---|---|---|---|
| BS1 | - | Control | - | 2 |
| BS2 | Cementitious | 2 | 0/90 | 1 |
| BS3 | Cementitious | 2 | 45/- 45 | 1 |

16

Only half of the beam was modelled in Abaqus taking into account the symmetry of the beam specimens. A roller support was created which had to be restricted for the displacement in the vertical direction. This translates as a roller support near the beam end. Symmetric boundary conditions were applied for the plane representing the continuation of the beam in reality. This included restriction of displacement in the corresponding horizontal direction and the rotation about the z-axis for this plane. Since the loading was displacement controlled, a plate loading was created which prevent stress concentration under the loading area throughout the duration of the test.

### 3.2 Comparison of experimental and numerical results.

The goal of the comparison of FE analysis results with the experimental test results is to ensure that the present finite-element model and analysis are capable of predicting the overall response of the RC beam strengthened with TRM composites. The results were compared through load-displacement behavior, Failure mode, and crack pattern. The numerical simulations agree well with test results as shown in Figure 9 including relation between ultimate load and maximum deflection at mid span, and in Figure 10 including failure modes of specimens respectively. Comparisons of experimental and numerical results are listed in Table 2.

**Table 2** Summary of the results of all verified beams.

| Specimen ID | Ultimate load (KN) | | | Mid-span deflection (mm) | | | Mode of failure | |
|---|---|---|---|---|---|---|---|---|
| | exp | num | exp/num | exp | num | exp/num | exp | num |
| **BS1** | 62.73 | 63.39 | 0.989 | 3.065 | 2.98 | 1.039 | Shear failure | Shear failure |
| **BS2** | 82.66 | 83.62 | 0.988 | 3.99 | 4.18 | 0.955 | Shear failure | Shear failure |
| **BS3** | 83.51 | 83.76 | 0.997 | 4.02 | 4.19 | 0.959 | Shear failure | Shear failure |

# 4 Parametric study

All of the specimens used for this study have the same overall cross-sectional dimensions of Al-Salloum et.al (2012) [14] control specimen (150 x 200 x1500 mm) as in Figure 8 and listed in Table 3. The 4-part nomenclature system, W-X-Y-Z has been used to identify each specimen. The W indicates the fiber type of TRM system (G for Glass, B for Basalt and C for Carbon), X represents the number of the textile layers, Y represents mortar type (C for cementitious mortar) and Z represents the thickness of the mortar. The roughness degree of the concrete substrate was assumed rough for all specimens and the interaction between the concrete and TRM composite was node-to-node interaction method using Cartesian connector element that is explained before.

### 4.1 Properties of Materials

### 4.1.1 Concrete and Steel Reinforcement

All of the specimens used for this study have the same cross section and reinforcement of Al-Salloum et.al(2012)[14] control specimen with average compressive strength, (fc') 15MPa. Poisson's ratio was assumed to be 0.20.

### 4.1.2 Mortar and textile

The properties of mortar and basalt fiber have the same properties of Al-Salloum et.al(2012)[14]. The properties of carbon and glass fiber are listed in Table 4.

## 5 Finite-Element Results and Discussion

In principle, the unstrengthened RC beam failed due to shear failure and that is attributed to diagonal tension cracks caused by shear stresses in the beam as shown in Figure 11(a). Most of the strengthened beams failed due to shear failure and the rest of specimens failed due de-ponding in the intersection between the beam and TRM as shown in Figure 11(b).

According to the results shown in Figure 12(a) and listed in Table 5, The ultimate load improved for specimens strengthened with Glass textile cementitious mortar, by increasing the number of layers, from 34.85% to 97.29% when using 2mm mortar thickness and it also increased from 46.29% to 97.14% by using 4mm mortar thickness.

According to the results shown in Figure 11(b) and listed in Table 5, The ultimate load

improved for specimens strengthened with carbon textile cementitious mortar by increasing the number of layers, from 54.90% to 90.63% when using 2mm mortar thickness and it also increased from 68.54% to 95.69% by using 4mm mortar thickness.

According to the results shown in Figure 11(c) and listed in Table 5, The ultimate load improved for specimens strengthened with Basalt textile cementitious mortar by increasing the number of layers, from 19.51% to 54.77% when using 2mm mortar thickness and it also increased from 39.82% to 88.97% by using 4mm mortar thickness.

**Table 4** Mechanical properties of carbon and glass textile.

| Fabric type | c/c spacing warp x weft (mm) | $A_f$ – warp ($mm^2$/ mm) | $A_f$ – weft ($mm^2$/ mm) | Elastic modulus (GPa) | Tensile strength (GPa) | Ultimate strain (%) |
|---|---|---|---|---|---|---|
| Carbon (C) | 10 × 10 | 0.0470 | 0.0470 | 240 | 4.8 | 1.8 |
| Glass (G) | 18 × 14 | 0.047 | 0.066 | 80 | 2.6 | 3.25 |

**Table 3 Test matrix of specimens.**

| Specimen ID | Strengthening details | | | | | | | | | | |
|---|---|---|---|---|---|---|---|---|---|---|---|
| | Textile details | | | | | Mortar details | | | | | |
| | Type | equ. thick. (mm) | no. of layers | $E_f$ (GPa) | Ffu (MPa) | type | Fc' (MPa) | Ft (MPa) | outer layer thick. (mm) | inner layer thick. (mm) | total thick per one side. (mm) |
| SCON | - | - | - | - | - | - | - | - | - | - | - |
| SC2C2 | carbon | 0.047 | 2 | 240 | 4800 | cementitious | 23.9 | 2 | 3 | 2 | 8 |
| SC4C2 | | | 4 | | | | | | 3 | 2 | 12 |
| SC6C2 | | | 6 | | | | | | 3 | 2 | 16 |
| SC2C4 | | | 2 | | | | | | 5 | 4 | 14 |
| SC4C4 | | | 4 | | | | | | 5 | 4 | 22 |
| SC6C4 | | | 6 | | | | | | 5 | 4 | 30 |
| SB2C2 | Basalt | 0.064 | 2 | 31.94 | 623 | cementitious | 23.9 | 2 | 3 | 2 | 8 |
| SB4C2 | | | 4 | | | | | | 3 | 2 | 12 |
| SB6C2 | | | 6 | | | | | | 3 | 2 | 16 |
| SB2C4 | | | 2 | | | | | | 5 | 4 | 14 |
| SB4C4 | | | 4 | | | | | | 5 | 4 | 22 |
| SB6C4 | | | 6 | | | | | | 5 | 4 | 30 |
| SG2C2 | Glass | 0.047 | 2 | 80 | 2600 | cementitious | 23.9 | 2 | 3 | 2 | 8 |
| SG4C2 | | | 4 | | | | | | 3 | 2 | 12 |
| SG6C2 | | | 6 | | | | | | 3 | 2 | 16 |
| SG2C4 | | | 2 | | | | | | 5 | 4 | 14 |
| SG4C4 | | | 4 | | | | | | 5 | 4 | 22 |
| SG6C4 | | | 6 | | | | | | 5 | 4 | 30 |

Ef: modulus of elasticity (GPa), Ffu: ultimate tensile stress of textile (MPa),
Fc' the compressive strength of mortar(Mpa),Ft the tensile strength of mortar (MPa).
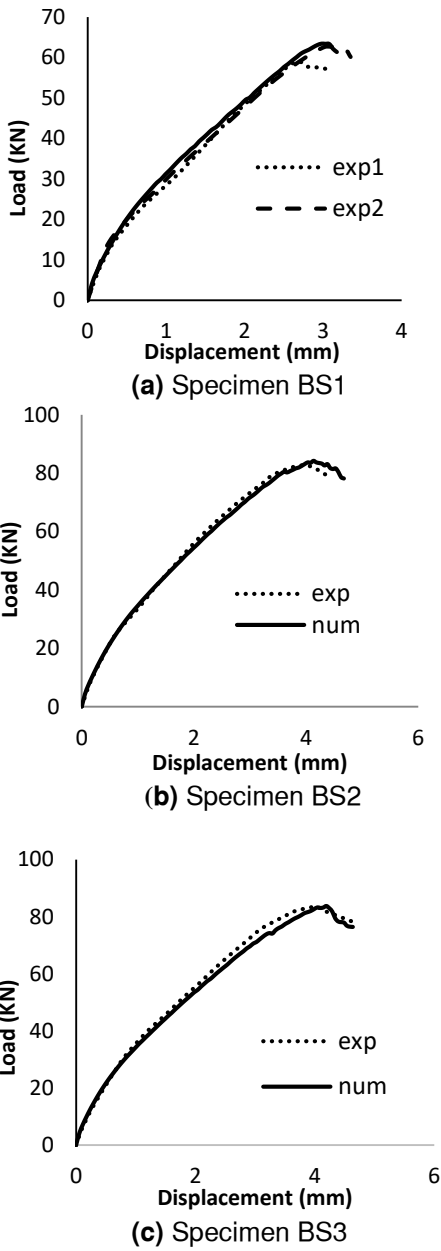
21

(a) Specimen BS1



(a)Failure mechanism of specimen BS1



(b) Specimen BS2



(b)Failure mechanism of specimen BS2



(c) Specimen BS3

**Figure 9** Load-displacement respose of shear specimens
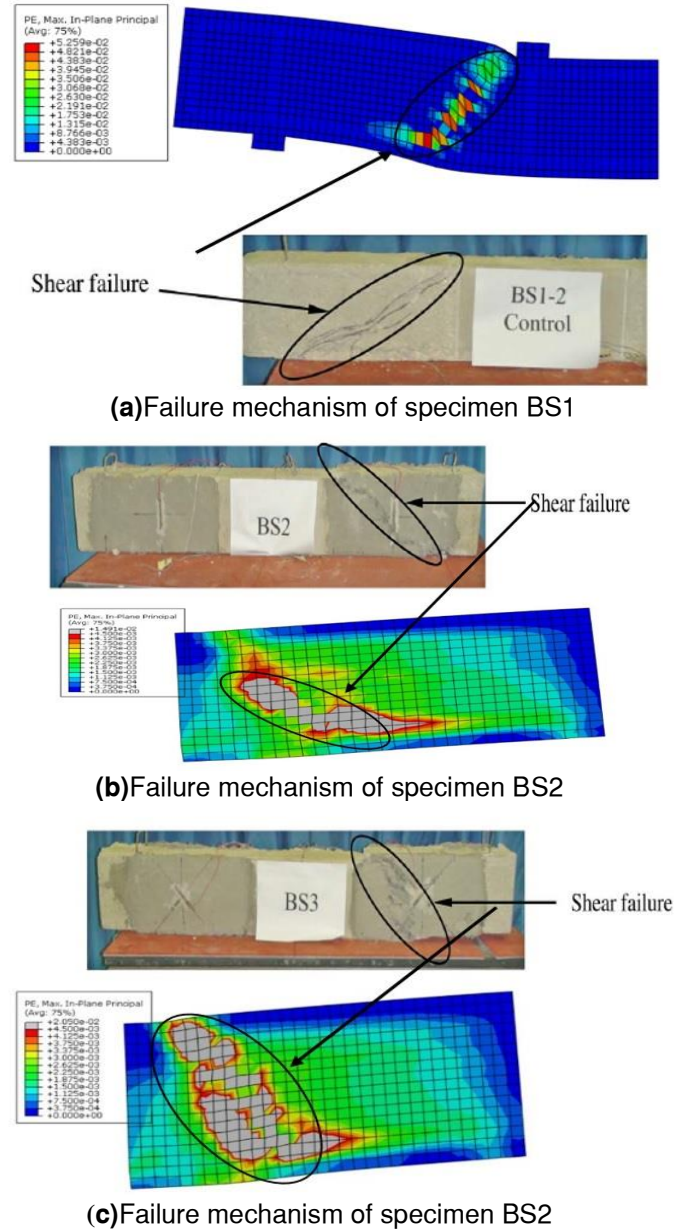


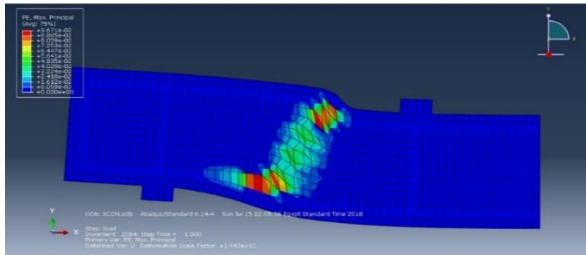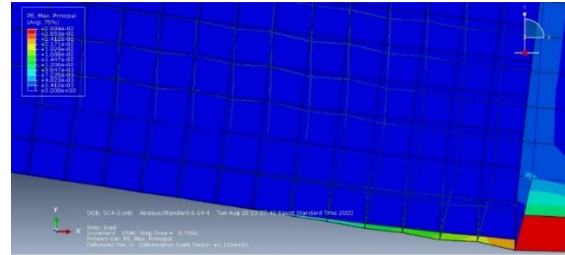(c)Failure mechanism of specimen BS2

**Figure 10** Failure mechanism of experimental versus numerical

**(a)** shear failure of control beam.



**(b)** de-bonding failure of strengthened specimens.

**Figure11** modes of failure of first group specimens.

**Table 5 results of specimens.**

| Specimen | Pu (KN) | Δ at Pu (mm) | % increase in Pu | Type of failure |
|----------|---------|--------------|------------------|-----------------|
| SCON | 58.2000 | 3.3228 | _____ | shear failure |
| SC2C2 | 90.1511 | 6.5504 | 54.90 | shear failure |
| SC4C2 | 102.8130 | 5.9000 | 76.65 | shear failure |
| SC6C2 | 110.9460 | 6.4171 | 90.63 | **De-bonding** |
| SC2C4 | 98.0903 | 7.1600 | 68.54 | shear failure |
| SC4C4 | 109.2110 | 6.4666 | 87.65 | shear failure |
| SC6C4 | 113.8930 | 5.8112 | 95.69 | **De-bonding** |
| SB2C2 | 69.5564 | 3.6501 | 19.51 | shear failure |
| SB4C2 | 77.8328 | 4.2674 | 33.73 | shear failure |
| SB6C2 | 90.0778 | 5.3483 | 54.77 | **De-bonding** |
| SB2C4 | 81.3748 | 4.7225 | 39.82 | shear failure |
| SB4C4 | 97.5879 | 6.2080 | 67.68 | shear failure |
| SB6C4 | 109.9790 | 6.4576 | 88.97 | **De-bonding** |
| SG2C2 | 78.4827 | 3.9117 | 34.85 | shear failure |
| SG4C2 | 88.9733 | 4.2132 | 52.88 | shear failure |
| SG6C2 | 114.82 | 7.6416 | 97.29 | **De-bonding** |
| SG2C4 | 85.138 | 4.004 | 46.29 | shear failure |
| SG4C4 | 106.733 | 5.967 | 83.39 | shear failure |
| SG6C4 | 114.736 | 6.590 | 97.14 | **De-bonding** |

Pu the ultimate peak load in (kn),  Δ the displacement at peak load in (mm)
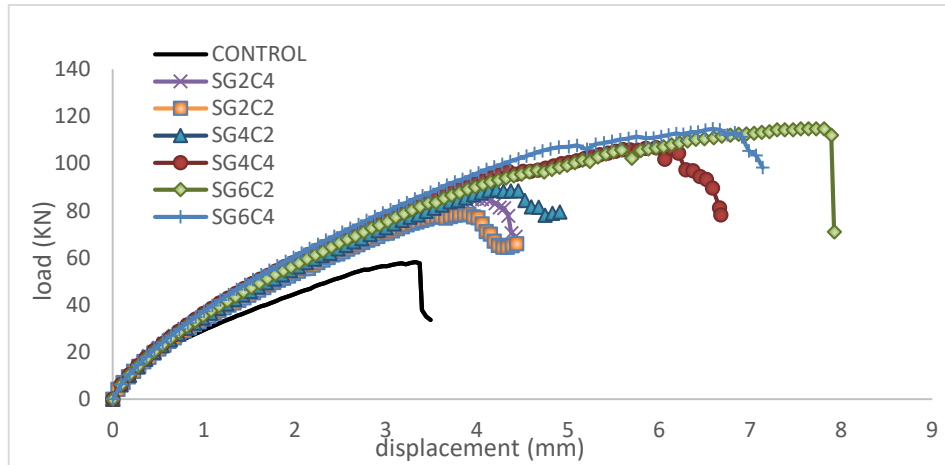
**(a)** Pu-Δ curves of specimens strengthened withGlass fibercementitious mortar.
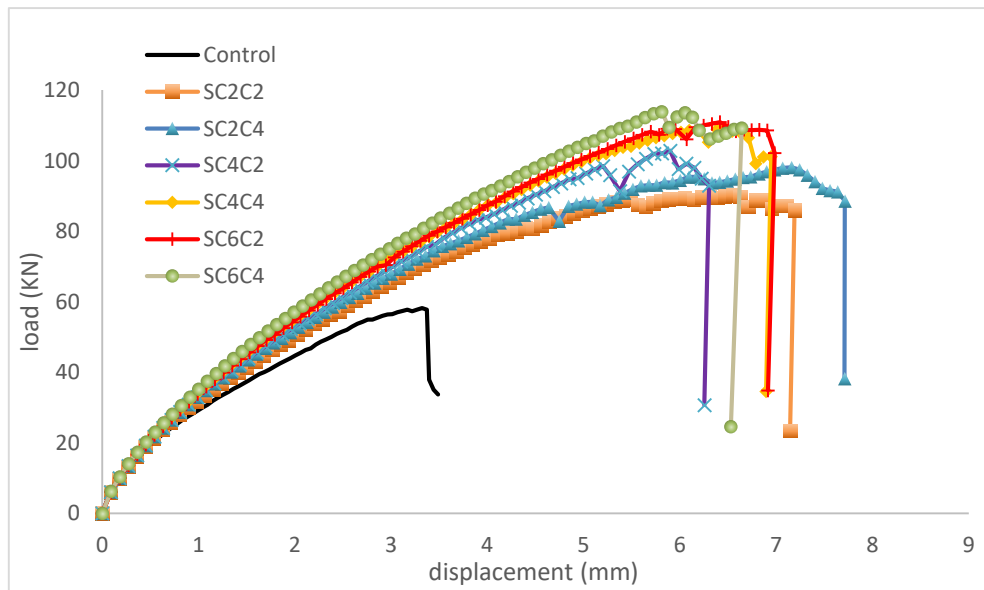


**(b)** Pu-Δ curves of specimens strengthened with carbon fiber cementitious mortar.
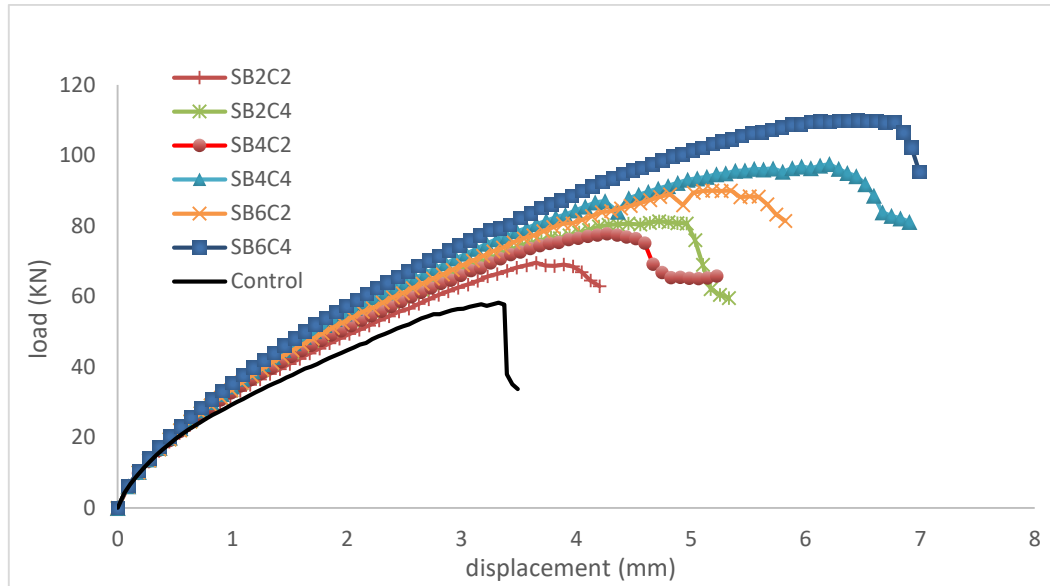
**(c)** Pu-Δ curves of specimens strengthened with Basalt fiber cementitious mortar.

**Figure 12** Pu-Δ curves of specimens.

# 6 Conclusions

On the basis of numerical results presented in this paper, the following conclusions can be drawn.

1. The 2D non-linear FEM can predict the overall behavior of RC beams strengthened with TRM with a good accuracy when compared with experimental results.

2. TRM provided substantial gain in the shear capacity and ductility of the RC beams. As anticipated, the shear resistance increased as the number of TRM layers increased from two to six layers per side and the mortar thickness increased from 2mm to 4mm.

3. Changing the number of layers, the fiber type and the mortar thickness may change the mode of failure. In detail, the failure of specimens (SG6C4, SC6C4 and SB6C4) moved to debonding, while the rest of specimens, the failure remains shear failure.

4. The FEM can show the de-bonding failure between TRM and concrete substrate and this depend on the bond-slip curve that can be obtained from single or double shear tests and the results are mainly affected by surface roughness.

## Declaration of conflicting interests

The author(s) declared no potential conflicts of interest with respect to the research, authorship, and/or publication of this article.

## Funding

### References

[1] fib bulletin 14. (2001). "Externally bonded FRP reinforcement for RC structures." Technical Rep. prepared by the Working Party EBR of Task Group 9.3, International Federation for Structural Concrete, Lausanne, Switzerland.

[2] Triantafillou, T. C., and Papanicolaou, C. G. (2006). "Shear strengthening of reinforced concrete members with textile reinforced mortar (TRM) jackets." Mater. Struct., 39(1), 93–103.

[3] Triantafillou, T. C., Papanicolaou, C. G., Zissimopoulos, P., and Laourdekis, T. (2006). "Concrete confinement with textile reinforced mortar (TRM) jackets." ACI Struct. J., 103(1), 28–37.

[4]    Peled, A., & Mobasher, B. (2007). Tensile behavior of fabric cement-based composites: pultruded and cast. Journal of Materials in Civil Engineering, 19(4), 340-348.

[5]    Contamine, R., Si Larbi, A., & Hamelin, P. (2011). Contribution to direct tensile testing of textile reinforced concrete (TRC) composites. Materials Science and Engineering: A, 528(29), 8589-8598.

[6]    Silva, F., Butler, M., Mechtcherine, V., Zhu, D., & Mobasher, B. (2011). Strain rate effect on the tensile behaviour of textile-reinforced concrete under static and dynamic loading. Materials Science and Engineering, A,528(3), 1727-1734.

[7]    Contamine, R., Junes, A., & Si Larbi, A. (2014). Tensile and in-plane shear behaviour

of textile reinforced concrete: Analysis of a new multiscale reinforcement. Construction and Building Materials, 51, 405-413.

[8]     Larrinaga, P., Chastre, C., Biscaia, H. C., & San-José, J. T. (2014). Experimental and numerical modeling of basalt textile reinforced mortar behavior under uniaxial tensile stress. Materials & Design, 55, 66-74.

[9]     Shams, A., Horstmann, M., & Hegger, J. (2014). Experimental investigations on textile-reinforced concrete (TRC) sandwich sections. Composite Structures, 118, 643-653

[10]    Colombo, I. G., Magri, A., Zani, G., Colombo, M., & Di Prisco, M. (2013). Erratum to: Textile Reinforced Concrete: experimental investigation on design parameters. Materials and structures, 46(11), 1953-1971.

[11]    Blänksvard, T., Täljsten, B., & Carolin, A. (2009). Shear strengthening of concrete structures with the use of mineral based composites. Journal of Composites for Construction, 13(1), 25-34.

[12]    Si Larbi, A., Contamine, R., Ferrier, E. & Hamelin, P. (2010). Shear strengthening of RC beams with textile reinforced concrete (TRC) plate. Construction and Building Materials, 24(10), 1928-1936.

[13] Adel Younis & usams A Ebead. (2018). Characterization and application of FRCM as a strengthening material for shear-critical RC beams. MATEC Web of Conferences 199, 09004 (2018).

 [14] Yousef A. Al-Salloum; Hussein M. Elsanadedy. (2012). Experimental and Numerical Study for the Shear Strengthening of Reinforced Concrete Beams Using Textile-Reinforced Mortar. Journal of Composites for Construction February 2012.

[15]    L. P. J. J. o. t. A. C. I. Saenz, "discussion of" Equation for the Stress-Strain Curve of Concrete" by Desayi and Krishnan," vol. 61, pp. 1229-1235, 1964.

[16]    H.-T. Hu and W. C. J. J. o. M. i. C. E. Schnobrich, "Constitutive modeling of concrete by using nonassociated plasticity," vol. 1, no. 4, pp. 199-216, 1989.

[17]    A. C. J. B. c. r. f. s. concrete and c. A. C. Institute, "American Concrete Institute, and International Organization for Standardization," 2008.

[18]    A. Hillerborg, M. Modéer, P.-E. J. C. Petersson, and c.research, "Analysis of crack formation and crack growth in concrete by means of fracture mechanics and finite elements," vol. 6, no. 6, pp. 773-781, 1976.

[19]    A. Hillerborg, M. Modéer, P.-E. J. C. Petersson, and c. research, "Analysis of crack

formation and crack growth in concrete by means of fracture mechanics and finite elements," vol. 6, no. 6, pp. 773-781, 1976.

[20]    W. D. Callister Jr and D. G. Rethwisch, Fundamentals of materials science and engineering: an integrated approach. John Wiley & Sons, 2012.

[21] D. S. J. D. S. Simulia, Providence, RI, "ABAQUS 6.13 User's manual,"vol. 305, p. 306, 2013.

[22] Mohammed A. Sakr, Ayman A. Sleemah, Tarek M. Khalifa, Walid N. Mansour (2019). Shear strengthening of reinforced concrete beams using prefabricated ultra-high performance fiber reinforced concrete plates: Experimental and numerical investigation. Journal of wiley. DOI: 10.1002/suco.201800137